Electronic Materials Letters, Vol. 1, No. 2 (2005), pp. 127-133

Measurement and Visualization of Doping Profile in Silicon Using Kelvin Probe Force Microscopy (KPFM)

Hyunjung Shin*, Bongki Lee, Chanhyung Kim, Hongsik Park[1], Dong-Ki Min[1], Juwhan Jung[1], and Seungbum Hong[1], and Sungdong Kim[2]

School of Advanced Materials Engineering, Kookmin University, Seoul 136-702, Korea
[1]Storage Laboratory, Samsung Advanced Institute of Technology, P.O Box 111, Suwon 440-600, Korea
[2]Seoul National University of Technology, School of Mechanical Design and Automation Engineering, Seoul 139-743, Korea

This paper demonstrates that Kelvin Probe Force Microscopy (KPFM) is applicable to the measurement of 2-D dopant profiles in silicon. By measuring contact potential differences, to the extent that this work-function difference is a consequence of dopant concentration at or near the sample surface, doping profiles are inferred from the measurement. Recently, scanning resistive probe microscopy (SRPM), a variant of SPM-based techniques, where a semiconductor resistor is located at the apex of the probe tip and surface charges can be observed directly, was proposed and developed. The spatial resolution of SRPM is dependent upon the size of the prepared resistor at the apex. The size of the resistor can be determined by the width (or channel) of the SiO_2 implant mask, where both sides of the mask in a p-type silicon substrate were opened, implanted with As^+ ions, and diffused by an activation process at 1000 ^oC for 10 to 16 hours. Using KPFM, we investigated doping profiles of the area of the resistor or, equivalently, underneath the mask. As annealing time was increased from 10 to 16 hours, shrinkage of the width (or channel) due to out-diffusion of implanted ions occurred. As a result, the contact potential difference between implanted n^+ and p (Si substrate) regions, which is equal to the resistive region, was decreased by increasing diffusion time. In conclusion, we showed that barrier height is lowered in the resisitive region, similar to a punch-through effect in a bipolar junction. It was also demonstrated that KPFM is a useful tool for measuring two-dimensional dopant profiles with nanometer spatial resolution.

Keywords: Kelvin probe force microscopy, scanning resistive probe microscopy, dopant profiles, space charge regions

1. INTRODUCTION

Recently, scanning resistive probe microscopy (SRPM)[1], a variant of SPM-based techniques, where a semiconducting resistor is located at the apex of the probe tip and surface charges can be observed directly, was newly proposed and fabricated. The working principle of detecting the surface charge is that resistance changes by the field induced in a small resistive region at the apex of the probe tip are measured. Details of the operation principle can be found in Ref. 1.

In terms of data storage, one of the advantages of SRPM over other SPM-based techniques is that no signal modulation or detection system is needed. Thus, scanning speed, a critical weakness in SPM-based data storage systems, could be dramatically enhanced. However, in order to render the SRPM technique a more compatible tool as a read/write head of a probe data storage system, higher spatial resolution and sensitivity are needed. In an SRPM system, a small resistive region at the apex of the tip determines the spatial resolution and sensitivity. Therefore, measurement of two-dimensional doping profiles in the resistive region is of critical importance.

Two-dimensional dopant profiling of semiconductor devices on a nanometer scale has long been an important challenge for material scientists and device engineers. To date, SIMS (secondary ion-mass spectroscopy), etching, and electron holography have been widely used for 2-D dopant profiling. However, all of these techniques are destructive. Conversely, Scanning Probe Microscopy (SPM) is a non-destructive technique, and has accordingly attracted much attention. Among the various SPM-based methodologies, scanning capacitance microscopy (SCM)[2,3], and scanning spreading resistance microscopy (SSRM)[4,5], are demonstrably powerful tools. However, using these techniques, it is

*Corresponding author: hjshin@kookmin.ac.kr

difficult to estimate the Fermi level in the doped region. In contrast, Kelvin Probe Force Microscopy (KPFM), a modified version of atomic force microscopy (AFM), can be effectively utilized to image 2D profiles of differences in the work functions of materials, depending on the dopant types and concentrations, in order to evaluate the Fermi level in a sub-100 nm scale doped region[6]. Consequently, KPFM has been employed in many diverse applications in just a few years. These applications include work function mapping[7,8], dopant profiling of semiconductor structures[9-12], imaging of heterojunctions[13], local surface potential mapping[14], and even electrical mapping for biological samples[15,16].

In practice, results obtained by KPFM should be interpreted in terms of effective surface potentials (effective contact potential differences, so-called electrochemical potential differences)[17,18], due to several other potential sources during KPFM readings. The sources can be broadly divided into two main contributions: stray capacitances from tip geometry and surface states. In an ideal case, it is assumed that all capacitance is due to the tip apex only. Practically, however, contributions from the tip-side-walls and from the cantilever itself can be very significant[19,20,21]. Therefore, the measured values of KPFM often differ from theoretical values, as reported by several authors[12-13, 19-24]. Hochwitz *et al*[22]. studied a model in which the main parasitic capacitance was due to cantilever-sample capacitance. Assuming clean surfaces without any contaminants such as oxides, isolated charges or condensed water films, Jacobs *et al.*[23,24], introduced weighted factors that correlate the measured potential with the actual surface potential distribution. They concluded that good resolution in potential maps is obtained by long and slender tips but not blunt ones.

In addition to the stray capacitances, another important source of potential differences between the measured and the theoretical values is the surface characteristics of materials, especially in semiconductors. Although surface characteristics are important phenomena, few studies of their influence on KPFM measurements have been reported relative to investigations on stray capacitances. In the case of semiconductor surfaces, Rosenwaks *et al.*[25] suggested that the lower built-in potential of the surface compared with that of bulk values in the *pn* junction of a GaP structure can explained by a depletion-type surface band bending effect. Specifically, the bands will be bent up in the n-doped region and down in the p-region, the net result being a reduction of surface built-in potential. Chavez-pirson *et al.*[13] also demonstrated that the effects of the surface states dramatically reduce the potential modulations of the *n-i-p-i* multiple quantum well (MQW) structure at the surfaces, resulting in a net modulation potential at surfaces of ~20 meV. Matsukawa *et al.*[12] estimated surface Fermi levels through passivation of surface states with thermally grown silicon oxide reducing the surface states. It was also reported[26,27], that a surface water layer, depending on the surface chemistry and atmospheric conditions, may shield the measured potential value, deteriorating the reliability of surface potential measurements and resulting in contrast degradation of potential.

In this work, in the process of fabricating a resistive probe, using KPFM we investigated doping profiles underneath a mask made as a resistive region in a resistive probe. Influences of the surface states and stray capacitance from the tip geometry on the measured potential by KPFM are also investigated.

2. EXPERIMENTAL PROCEDURE

Electric force, F, given by the derivative of the electrical energy acting on the tip when an electric field between the tip and sample is applied, is described below

$$F = \frac{1}{2}\frac{\partial C}{\partial z}V^2 \tag{1}$$

where V is the voltage applied between the tip and the portion of the sample beneath it, z is the average tip-sample distance, and $\partial C/\partial z$ is the change in tip-sample capacitance due to the tip oscillation. In order to create electrostatic force, modulation of superimposition of ac and dc voltages should be applied. The applied voltage, $V=V_{dc}+V_{ac}sin(\omega t)$, yields

$$F = \frac{1}{2}\frac{\partial C}{\partial z}\left[V_{dc}^2 + \frac{1}{2}V_{ac} + 2V_{dc}V_{ac}sin(\omega t) - \frac{1}{2}V_{ac}^2 cos(2\omega t)\right]$$
$$= F_{dc} + F_{1\omega} + F_{2\omega} \tag{2}$$

with spectral components at the dc, ω, and 2ω components. Note that the amplitude of the vibration of the tip at the frequency ω is proportional to V_{dc}. V_{dc} includes the contact potential difference between the tip and sample and external dc voltages (i.e., offset voltage), which are given by

$$V_{dc} = V_{CPD} - V_{ext} = (\phi_m - \chi_{Si} - \Delta E_{fn} - \Delta\phi) - V_{exi} \tag{3}$$

Here, $Ø_m$ is the metal work function of the tip, χ_{Si} is the electron affinity of Si, ΔE_{fn} is the bulk Fermi level in Si relative to the conduction band edge, and ΔØ is the surface band bending due to the surface states. The contact potential difference, V_{CPD}, is then obtained by the following procedure: a lock-in amp allows extraction of the first harmonic of tip deflection. A feedback loop is employed to maintain it equal to zero by adjusting V_{ext}; the external voltage (dc) is varied until the alternating current (ac) vibration of the tip at the frequency ω is nullified. Clearly, the condition $F_\omega = 0$ is achieved when V_{ext} is equal to V_{CPD}. Thus, the contact potential difference is directly measured by adjusting the potential offset on the tip and keeping the first harmonic response zeroed. In the ideal case, the signal measured is independent of the geometric properties of the tip-surface system and the modulation voltages[28]. A typical set-up for KPFM is sche-

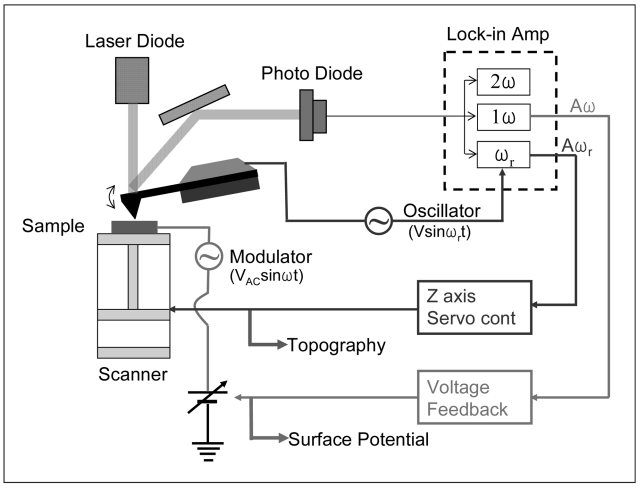

Fig. 1. Schematic diagram of the KPFM measurement setup. Signal for topography is shown with a blue line and that for the CPD is shown with a red line.

matically shown in Fig. 1.

Resistive patterns were prepared by the following procedure. Doping concentration of the p-type silicon substrate is set at approximately 1×10^{15} cm^{-3}. In Fig. 2(a), thermal oxides are employed as implantation mask layers. Regions of n^+ were formed by implantation with arsenic ions (1×10^{16} cm^{-2}, 300 KeV), followed by annealing for activation and diffusion of the ions at 1000 °C for 10~16 hrs. During annealing, implanted arsenic ions are diffused into p-Si under the mask where a resistive region is formed, as shown schematically in Fig. 2(b). Prior to KPFM measurements, the resistive patterns were exposed by buffered oxide enchant (BOE) so as to remove surface contaminants as well as thermal oxide layers. The samples were heated for 1h at 150 °C to remove the surface water adsorbed layers. All measurements of KPFM were performed using commercial Scanning Probe Microscopy (SPA400 and SPI 4000 from Seiko Instruments) employing a $PtIr_5$ coated Si cantilever

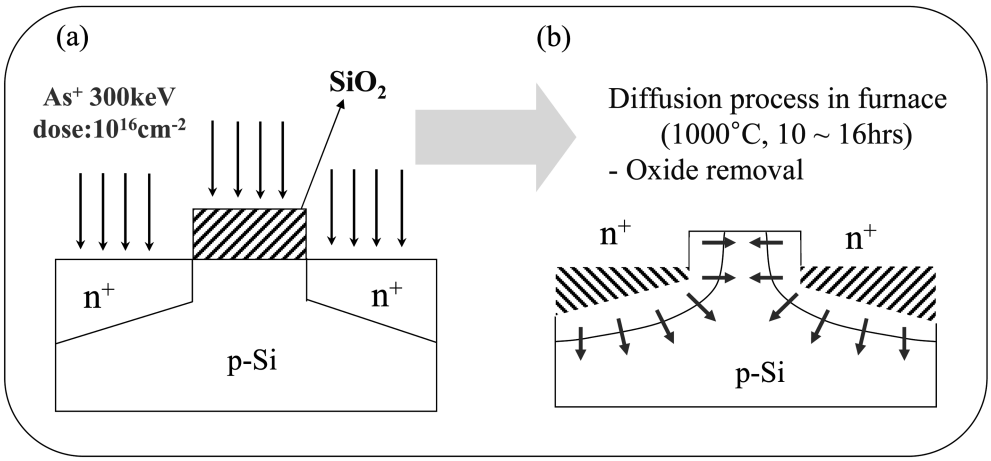

Fig. 2. (a) and (b) Schematic diagram of experimental procedure: (a) Ion implantation of As^+ ions; (b) annealing process for activation and diffusion of As^+ ion at 1000 °C for 10 ~ 16 hrs.

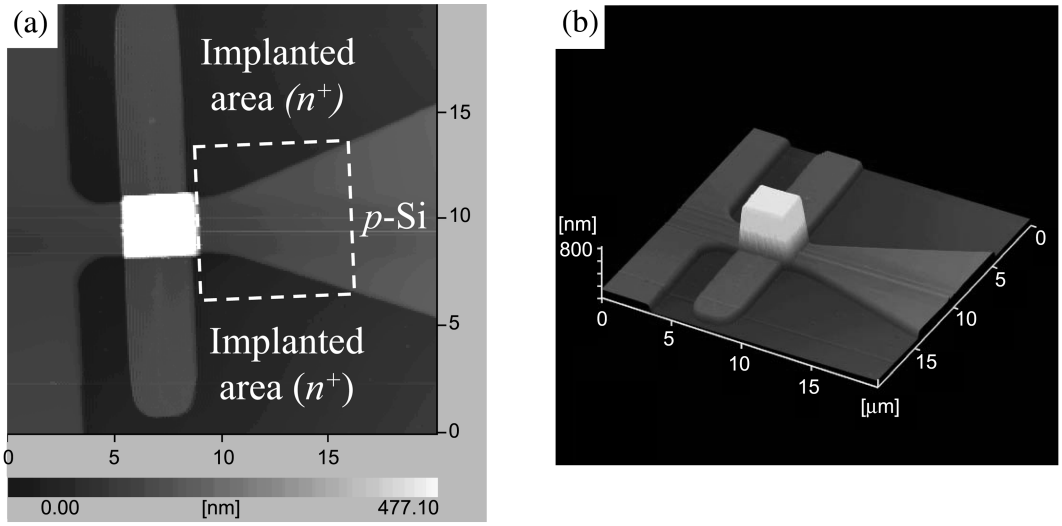

Fig. 3. (a) and (b) (Color) The overall topography: two- (a) and three- (b) dimensional images of a resistive pattern.

with a spring constant of ~2 N/m. Resonance frequency and Q-factor of the cantilever were approximately 60 KHz and 170, respectively. AC voltage of 6~7 V_{p-p} at a frequency of 25 KHz was applied between the probe and the sample. KPFM images of the sample surfaces were acquired at a probe scan rate of 0.2 Hz. All measurements were conducted in ambient conditions.

3. RESULTS AND DISCUSSION

The resulting overall three-dimensional topography of the resistive pattern is shown in Fig. 3(b). Fig. 3(a) shows the resistive pattern, indicating the *p*- and n^+ - type regions with the implanted area of As^+ ions. The most protruded region in Fig. 3(a) is the etching mask for the tip. KPFM measurements have been performed for dopant profiling of area boxed by dash lines in Fig. 3(a). During the annealing process the implanted regions expanded diffusively into the p-Si substrate, and resistive regions were consequently formed.

The results in Figs. 4(a) and (b) are taken from the sample annealed at 1000 °C for 12 hours. Figures 4(a) and (b) show topography and potential images of the resistive pattern in

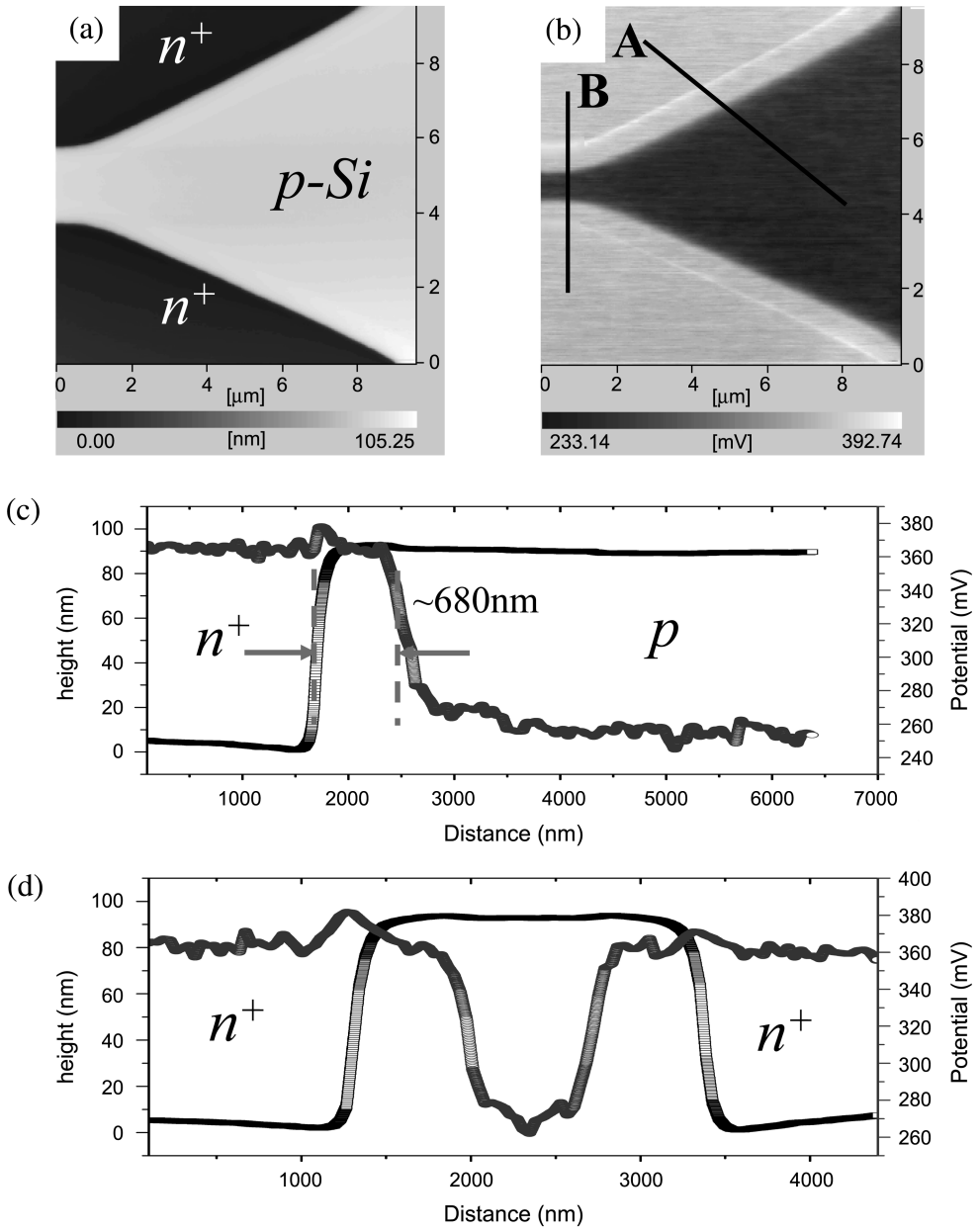

Fig. 4. (a) and (b) (color) (a) topography and (b) potential images were taken simultaneously by non-contact and KPFM on a resistive pattern in equilibrium. A cross-sectional line diagram (c) and (d) of lines A and B in Fig. 4(b), respectively. (Black line and blue line represent the measured potential and topography, respectively.)

equilibrium, respectively. Brighter contrast (higher potential values) was observed in the n^+ regions than in the surrounding p regions, as shown in Fig. 4(b). Considering the principle of KPFM measurement (the measured potential corresponds to the work function difference between the tip and the sample), the contact potential difference of an ideal *pn* junction should yield a higher potential for the n-region, which is consistent with our results[29]. However, in most reports on KPFM measurements for Si *pn* junctions, the potential of *p*-regions is higher than that of *n*-regions[9-11]. At present, there is no clear explanation for the discrepancy between the results of previous reports and theoretical predictions[30].

Figure 4(c) also shows that the maximum difference in potentials (line A in Fig. 4(b)) is approximately 120 mV, which is lower than the value calculated from the doping levels of n^+ and *p*-Si (about 813 mV). A probable explanation for this discrepancy is as follows. In the introduction it was noted that several sources give rise to potential differences between the measured and the theoretical values: surface states and stray capacitances. In practice, they both influence KPFM measurements. In the case of semiconductor surfaces, the surface states contributed more to the measured potentials than the stray capacitance. In order to study the effects of the surface states on reading the potentials by KPFM in a semiconductor, the dependencies of the first harmonic signal on *dc* are investigated. Specifically, the minimum value of the amplitude of the first harmonic function of applied *dc* bias was determined.[31,32] Figure 5(a) shows the measured amplitude of the first harmonic signal in the electrostatic force on Pt (111) and Au (111) film surfaces, respectively, as a function of the *dc* offset in the sample bias. The *dc* offset at which the amplitude of the first harmonic signal is minimal indicates the contact potential difference between the tip and sample. The contact potential differences between the tip and Pt and Au films were approximately 0.12V and -0.16 V, respectively, as shown in Fig. 5(a). The measured potential difference between Pt and Au films is about ~0.28 V, displaying excellent agreement with the published data, taking into account the contact potential difference between Pt (111) (5.6~7 eV) and Au (111) (5.3~5.35 eV) films . On the other hand, in the case of a semiconductor, the measured value with the same procedure as that employed for Fig. 5(a) was ~0.38 V, as shown in Fig. 5(b), although the contact potential difference between n+ and p-Si is about 0.8~0.9 V when calculated by doping type and concentration. Assuming that the contributions of stray capacitances are constant in both cases (i.e., flat surface, tip geometry, and distance between tip and sample are identical), the difference between the measured and theoretical values in the semiconductor could be explained by the effect of the surface states. Consequently, in the case of the semiconductor, the surface states are more effective on the surface potential, which is measured by KPFM.

It was clearly demonstrated that the implanted area is expanded diffusively into p-Si due to the annealing process (about ~680 nm), as shown in Fig. 4(c). In this sample, since the doping level in the n^+-type region (1×10^{19}/cm^3) is much higher than that in the *p*-type region (1×10^{15}/cm^3), almost all the depletion regions will be formed in the p-Si substrates. Figure 4(c) indicates that the measured potential drop extends over the *p*-Si. In Fig. 4(d), however, a cross-sectional potential profile (blue line) of line B (a so-called channel) in Fig. 4(b) indicates the *p*-region does not have sufficient physical length to form complete depletion due to the diffusion of arsenic ions for the annealing process.

Figure 6(b) presents the potential line profile corresponding to each line (*A*, *B*, *C*, and *D*) in Fig. 6(a). As As^+ ions dif-

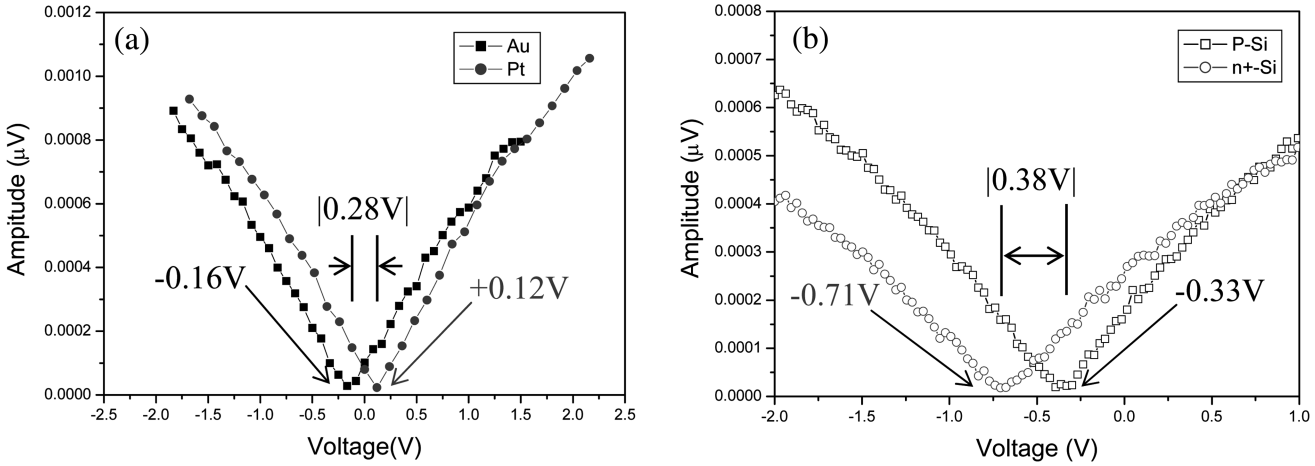

Fig. 5. (a) and (b) (Color) Measured amplitudes of electrostatic force at first harmonic signal on (a) Pt(111) (red line) and Au(111) (black line) film (b) *p*-Si substrate (black line) and n^+- Si substrate (red line) as a function of the *dc* offset. ac bias of 1 V_{RMS} at 27 KHz was applied and a $PtIr_5$ tip was used. The semiconductor samples were a p-type Si wafer with [100] orientation covered with 50 nm thick thermally grown SiO_2 and a heavily doped n^+-type wafer covered with native oxide.

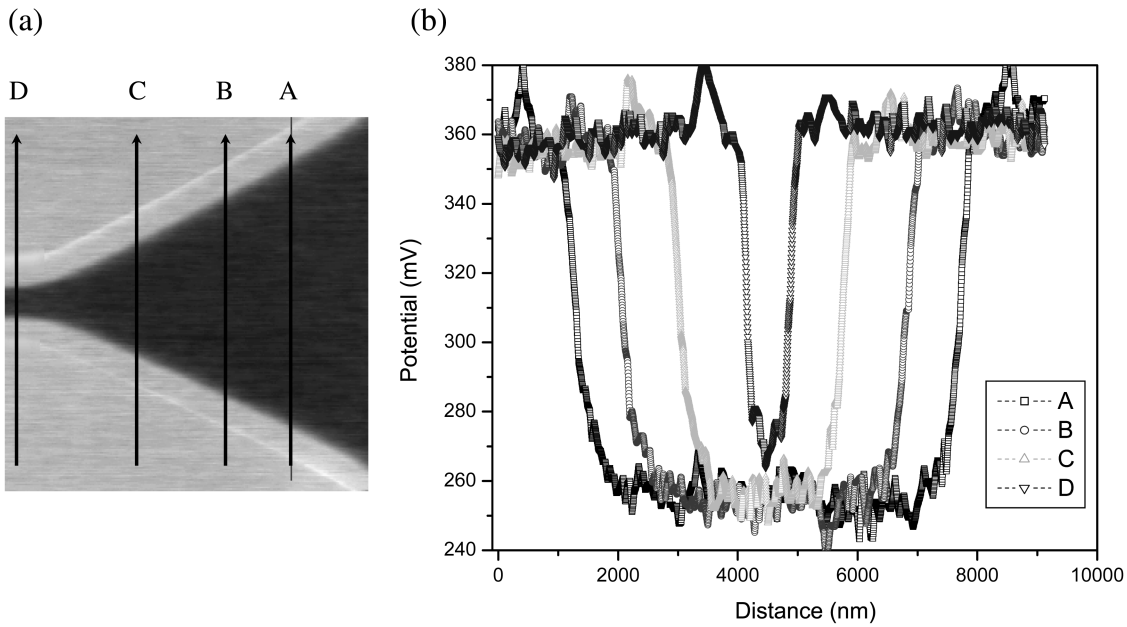

Fig. 6. (a) and (b) (Color) Potential image (a) for annealing for 12 hours (b) cross-sectional potential line diagrams as a function of position with A, B, C, and D, respectively

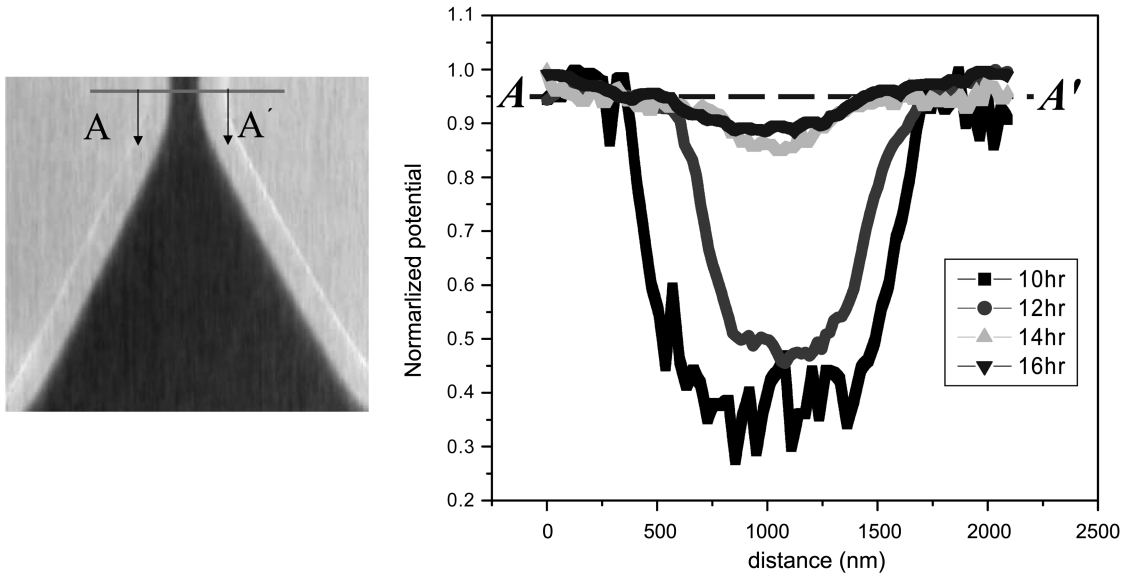

Fig. 7. (Color) Normalized potential line profiles across the resistive region as a function of annealing time from 10 to 16 hours.

fuse, the depletion layers extend from each n^+ region into the channel, and thus the width of the neutral *p*-region was decreased. The potential differences of the channel region indicated by line *D* are smaller than those of line *A*, *B*, and *C* because the channel region, that is line *D*, does not have enough physical space to form a complete depletion region.

Figure 7 shows normalized potential profiles of cross-sectional resistive regions (i.e., channels) as a function of annealing time from 10 to 16hrs. The potential differences of the $n^+/p/n^+$ junction decreased with increasing annealing time, implying that the implanted arsenic ions are diffused into the p-region. Since the resistive region (channel) was depleted for 12 hours, the resistive region may be converted into *n*-type with an annealing time of 14 to 16 hours, as shown in Fig. 7. Finally, the entire channel was depleted, showing a *punch-through effect* in the bipolar junction. In order to verify that the ions overlap, we also performed electrical current - voltage (I-V) measurements with test diffusion patterns having different channel widths (1.6 ~ 4 μm) and various annealing times (8 ~ 16 hours) at a fixed anneal-

ing temperature of 1000 °C. Linear I-V characteristics, i.e., ohmic behaviors, have been observed at widths smaller than 2 μm. With the mask width fixed at 2 μm, the ohmic behaviors were found in the samples annealed for 12, 14, and 16 hours, having the same resistance of approximately 100 Ω. In contrast, the I-V characteristics of the remaining samples showing nonlinear I-V characteristics are ascribed to the leakage current through the overlapped SCRs and the saturation of drift-velocity in the higher electric field. In order to form a resistive region in the apex of the tip, the relative differences between the resistive regions and the reference in the normalized CPDs should be more than 20%. Figure 7 indicates that the resulting resistance probe should be devised as a JFET (Junction Field-Effect Transistor) in the apex of the tip, sensing resistance changes upon the external electric field - working principle of the SRPM.

4. CONCLUSIONS

In conclusion, SRPM shows potential as a read/write head of probe storage devices because of its unique functionality. Prior to the fabrication of the resistive probe we demonstrated the use of KPFM for two-dimensional potential mapping in equilibrium. The surface potential distribution at the *pn* junction exhibited contrast consistent with the order of the bulk Fermi level. In the KPFM measurement, in the case of a semiconductor, surface characteristics were found to be more effective for potential measurement than stray capacitances.

ACKNOWLEDGEMENTS

The authors would like to express their appreciation for financial support from Samsung Electronics, Co., a research grant (R-01-2005-000-11172-0) from Korea Science & Engineering Foundation, AOARD (Asian Office of Aerospace Research and Development; FA5209-05-P-0350), and the SRC/ERC program of MOST/KOSEF (grant #R11-2005-048-00000-0).

REFERENCES

1. H. Park, J. Jung, D.-K. Min, S. Kim, S. Hong, and H. Shin, *Appl. Phys. Lett.* **84**, 1734 (2004).
2. N. Nakagiri, T. Yamamoto, H. Sugimura, Y. Suzuki, M. Miyashita, and S. Watanabe, *Nanotechnology* **8**, A32 (1999).
3. C. Y. Nakakura, D. L. Hetherington, M. R. Shaneyflet, P. J. Shea, and A. N. Erickson, *Appl. Phys. Lett.* **75**, 2319 (1999).
4. P. De Wolf, T. Clarysse, W. Vandervorst, L. Hellemans, Ph. Niedermann, and W. Hanni, *J. Vac. Sci. Technol. B* **16**, 401 (1998).
5. P. De Wolf, R. Stephenson, T. Trenkler, T. Clarysse, T. Hantschel, and W. Vandervorst, *J. Vac. Sci. Technol. B* **18**, 361 (2000).
6. H. Fujii, S. Kanemaru, T. Matsukawa, and J. Itoh, *Appl. Phys. Lett.* **78**, 2560 (2001).
7. H. O. Jacobs, H. F. Knapp, S. Muller, A. Stemmer, *Ultramicroscopy* **69**, 39 (1997).
8. M. Nonnenmacher, M. P. O'Boyle, and H. K. Wickramasinghe, *Appl. Phys. Lett*. **58**, 2921 (1991).
9. A. Kikukawa, S. Hosaka, and R. Imura, *Appl. Phys. Lett*. **77**, 2358 (1995).
10. A. K. Henning and T. Hochwitz, *J. Appl. Phys.* **77**, 1888 (1995).
11. M. Tanimoto and O. Vatel, *J. Vac. Technol. B* **14** 1547 (1996).
12. T. Matsukawa, S. Kanemaru, M. Masahara, M. Nagao, H. Tanoue, and J. Itoh, *Appl. Phys. Lett.* **82**, 2166 (2003).
13. A. Chavez-Pirson, O. Vatel, M. Tanimoto, H. Ando, H. Iwamura, and H. Kanbe, *Appl. Phys. Lett.* **67**, 2358 (1995).
14. D. W. Abraham and H. K. Wichramasinghe, *J. Vac. Sci. Technol. B* **9**, 1559 (1991).
15. M. Fujihira and H. Kawate, *J. Vac. Sci. Technol. B* **12**, 1604 (1994).
16. S. Yamashina and M. Shigeno, *J. Electron. Microsc.* **44,** 462 (1995).
17. S. V. Kalinin and D. A. Bennell, *Phys. Rev. B* **62**, 10419, (2000).
18. A. K. Henning, T. Hochwitz, J. Slinkman, J. Never, S. Hoffmann, P. Kaszuba, and C. Daghlian, *J. Appl. Phys.* **77**, 1888 (1995).
19. G. Koley, M. G. Spencer, and H. R. Bhangale, *Appl. Phys. Lett.* **79**, 545 (2001).
20. S. G. Monivas, L. S. Froufe, R. Carminati, J. J. Greffet, and J. J. Saenz, *Nanotechnology* **12**, 496 (2001).
21. S. Hudlet, M. S. Jean, C. Guthmann, and J. Berger, *Eur. Phys. J. B* **2**, 5 (1998).
22. T. Hochwitz, A. K. Henning, C. Lewey, C. Daghlian, and J. Slinkman, *J. Vac. Sci. Technol. B* **14**, 457 (1996).
23. H. O. Jacobs, P. L. Euchtmann, O. J. Homan, and A. Stemmer, *J. Appl. Phys.* **84**, 1168 (1998).
24. H. O. Jacobs and A. Stemmer, *Surf. Interface Anal.* **27**, 361 (1999).
25. R. Shikler, T. Meoded, N. Fried, B. Michori, and Y. Rosenwarks, *J. Appl. Phys.* **86**, 107 (1999).
26. H. Sugimura, Y. Ishida, K. Hayashi, O. Takai, and N. Nakagiri, *Appl. Phys. Lett.* **80**, 1459 (2002).
27. S. Ono, M. Takeushi, and T. Takahashi, *Appl. Phys. Lett.* **78**, 1086 (2001).
28. Edited by D. A. Bonnell "*Scanning Probe Microscopy and Spectroscopy: Theory, Techniques, and Applications*" 2nd, Wiley-VCH (2001).
29. S. M. Sze, "*Physics of semiconductor Devices*", 2nd ed, Wiley, New York (1981).
30. T. Mizutani, T. Usunami, S. Kishimoto, and K. Maezawa. *Jpn. J. Appl. Phys.* **38**, 4893 (1999).
31. S. Hong, J. Woo, H. Shin, J.-U. Jeon, Y. E. Park, E. L. Colla, N. Setter, E. Kim, and K. No, *J. Appl. Phys.* ***89***, 1377 (2001).
32. T. Takahashi and T. Kawamukai, *Ultramicroscopy* **82**, 63 (2000).
33. *Handbook of Chemistry and Physics* (ed., D. R. Lide), CRC Press, FL (1995).